

Constrained flow around a magnetic obstacle

EVGENY V. VOTYAKOV¹†, EGBERT ZIENICKE¹
AND YURI B. KOLESNIKOV²

¹Institut für Physik, Technische Universität Ilmenau, PF 100565, 98684 Ilmenau, Germany

²Fakultät Maschinenbau, Technische Universität Ilmenau, PF 100565, 98684 Ilmenau, Germany

(Received 27 April 2007 and in revised form 7 May 2008)

Many practical applications exploit an external local magnetic field – magnetic obstacle – as an essential part of their operation. It has been demonstrated that the flow of an electrically conducting fluid influenced by an external field can show several kinds of recirculation. The present paper reports a three-dimensional numerical study, some results of which are compared with an experiment on such a flow in a rectangular duct. First, we derive equations to compute analytically the external magnetic field and verify these equations by comparing with experimentally measured field intensity. Then, we study flow characteristics for different magnetic field configurations. The flow inside the magnetic gap is dependent mainly on the interaction parameter N , which represents the ratio of the Lorentz force to the inertial force. Depending on the constraint factor $\kappa = M_y/L_y$, where M_y and L_y are the half-widths of the external magnet and duct, the flow can show different stationary recirculation patterns: two magnetic vortices at small κ , a six-vortex ensemble at moderate κ , and no vortices at large κ . Recirculation appears when N is higher than a critical value $N_{c,m}$. The driving force for the recirculation is the reverse electromotive force that arises to balance the reverse electrostatic field. The reversal of the electrostatic field is caused by the concurrence of internal and external vorticity respectively related to the internal and external slopes in the M-shaped velocity profile. The critical value of $N_{c,m}$ grows quickly as κ increases. For the case of well-developed recirculation, the numerical reverse velocity agrees well with that obtained in experiments. Two different magnetic systems can induce the same electric field and stagnation region provided these systems have the same power of recirculation, given by the $N/N_{c,m}$ ratio. The three-dimensional helical characteristics of the vortices are elaborated, and an analogy is shown to exist between helical motion inside the recirculation studied and secondary motion in Ekman pumping. Finally, it is shown that a two-dimensional model fails to properly produce stable two- and six-vortex structures as found in the three-dimensional system. Interestingly, these recirculation patterns appear only as time-dependent and unstable transitional states before a Kármán vortex street forms, when one suddenly applies a retarding local magnetic field to a constant flow.

1. Introduction

An electrically conducting fluid flow influenced by a local external magnetic field is of considerable fundamental and practical interest. When applied to the flow, a transverse homogeneous magnetic field creates a so-called magnetic obstacle, i.e. a region where the flow motion is retarded by the Lorentz force.

† Current address: University of Cyprus, 75 Kallipoleos Avenue, P.O. Box 20537, 1678 Nicosia, Cyprus.

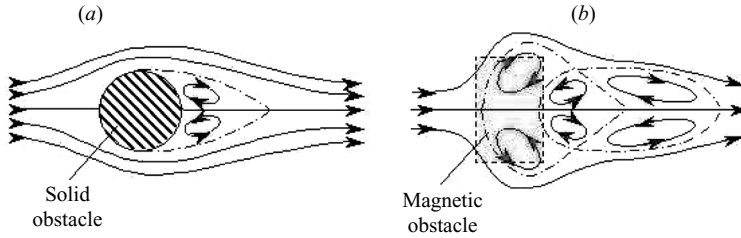


FIGURE 1. Structure of the wake of a solid (a) and magnetic obstacle (b). By forming the wake, the solid obstacle develops attached vortices, while the magnetic obstacle develops inner (first pair), connecting (second) and attached vortices (third pair).

On the fundamental side, such a system possesses a rich variety of dynamical states. This is because its behaviour is characterized by two parameters, the Reynolds number $Re = u_0 H / \nu$ and interaction parameter $N = \sigma H B_0^2 / \rho u_0$, where H , u_0 , B_0 are characteristic scale, velocity and magnetic field induction, and ρ , ν , σ are density, kinematic viscosity, and electric conductivity of the fluid, see e.g. Shercliff (1962), Roberts (1967), Moreau (1990), Davidson (2001). Re represents the ratio of the inertial to viscous forces in the flow, and N represents the ratio of the Lorentz forces to the inertial forces. In ordinary hydrodynamics, such as the flow around a solid obstacle, an increase of the inertial force, i.e. Re , introduces the nonlinear dynamics characterized by a vortex motion past the obstacle, see figure 1(a). The additional flow parameter N brings new nonlinear degrees of freedom to the problem as elaborated recently by Votyakov *et al.* (2007), see figure 1(b).

On the practical side, spatially localized magnetic fields play an essential role in a variety of industrial applications in metallurgy, see e.g. Davidson (1999), including stirring of melts by a moving magnetic obstacle (called electromagnetic stirring, e.g. Kunstreich 2003), removing undesired turbulent fluctuations during steel casting using steady magnetic obstacles (called electromagnetic braking, e.g. Takeuchi *et al.* 2003) and non-contact flow measurement using a magnetic obstacle (called Lorentz force velocimetry, e.g. Thess, Votyakov & Kolesnikov 2006). For instance, it is important to understand whether the useful turbulence-damping effect of a magnetic brake is obliterated by excessive vorticity generation in the wake of the magnetic obstacle.

As is well known, in the flow past a solid obstacle, there is a stagnation region where one can observe a recirculation in the appropriate Reynolds number regime, so-called attached vortices shown in figure 1(a). If the solid obstacle is replaced by a magnetic obstacle, by means of a local external magnetic field, then electrical eddy currents \mathbf{j} will appear which induce the Lorentz force $\mathbf{F}_L = \mathbf{j} \times \mathbf{B}$. The largest retarding effect occurs where the transverse magnetic field \mathbf{B} is a maximum. Therefore, past the magnetic obstacle there is also a stagnation region where a kind of a reverse flow might be obtained. This analogy between a solid and a magnetic obstacle has been known from the beginning of magnetohydrodynamics (MHD). In the earliest two-dimensional numerical simulation, Gelfgat, Peterson & Shcherbinin (1978) observed a kind of recirculation and noted the analogy with a solid body: ‘the qualitative pattern of the streamlines in such a flow is similar to the situation which arises in the case of the flow around objects’. However, the specially designed physical experiments of Gelfgat & Olshanskii (1978) following this simulation failed to confirm their previous numerical results: ‘special attempts which we made to detect zones with return flow were not successful. The negative flows which occur in certain numerical calculations

are obviously due to inaccuracies in the calculation'. They were correct about the inaccuracies of their two-dimensional approach in the sense that this approach is not suitable to describe their experiments; nevertheless it has still been possible to reveal a kind of recirculation in the experiments. We shall discuss this later in the §3.2.

For Western readers, the term 'magnetic obstacle' was revived in Cuevas, Smolentsev & Abdou (2006a). (In the 1970s, one of the authors, Yu. K., used 'magnetic obstacle' as a working term in the Riga, MHD centre of the former USSR.) Cuevas *et al.* (2006a) performed a two-dimensional numerical study and described a Kármán vortex street past the obstacle similar to those observed past a circular solid cylinder. We discuss the link between our three-dimensional stationary and their two-dimensional non-stationary results in §3.7.

The most recent results on the wake of a magnetic obstacle have been obtained by Votyakov *et al.* (2007). Their main result is presented in figure 1 where the qualitative structure of the wake of a magnetic obstacle is given in comparison with the wake of a physical obstacle. By means of three-dimensional simulation and experiments, Votyakov *et al.* (2007) found that the liquid metal flow shows three different regimes: (i) no vortices, when the viscous force prevails at small Lorentz force, (ii) one pair of *inner magnetic* vortices between the magnetic poles, when the Lorentz force is high and inertia small, and (iii) three pairs, namely, magnetic as in (ii), plus *connecting* and *attached* vortices, when the Lorentz and inertial forces are high. The latter six-vortex ensemble is shown in figure 1(b).

An important factor in the flow influenced by an external magnetic field is the spanwise heterogeneity of the field. One can distinguish two extremal cases: (i) a pointwise braking Lorentz force, and (ii) a spanwise homogeneous braking Lorentz force. The latter case can be easily created, e.g. by external magnets long enough to overlap the duct, while the first case represents an idealization since it is impossible to have a pointwise external magnetic field. The first case is well-studied in a two-dimensional stratified flow, e.g. Voropayev & Afanasyev (1994); it has been shown that dipolar vorticity is generated in the vicinity of the origin of the point braking force. Applied to MHD flows, similar results were obtained with a two-dimensional numerical simulation of creeping flow both by Gelfgat *et al.* (1978) and recently by Cuevas, Smolentsev & Abdou (2006b). The vortex dipole observed in those works is of the same nature as the magnetic vortices that we will discuss in the present paper.

The second case, spanwise homogeneous magnetic fields, is of traditional MHD interest and well understood. In particular, an M-shaped profile is developed under a streamwise magnetic field gradient, Shercliff (1962). It has been studied extensively in experiments (Kit *et al.* 1970; Tananaev 1979) and by numerical simulation (Sterl 1990; Votyakov & Zienicke 2007). The most recent numerical paper (Votyakov & Zienicke 2007) by comparing with experiment (Andreev, Kolesnikov & Thess 2007) has established that when turbulent pulsations are suppressed by an external magnetic field, the interaction parameter N governs the flow. It has been shown numerically that a spanwise homogeneous magnetic field is not able to reverse the electric field inside the magnetic gap. As we shall prove below spanwise inhomogeneity is a necessary condition to induce recirculation between magnetic poles.

The goals of the present paper are the following: (i) to report details not published in Votyakov *et al.* (2007) (ii) to investigate thoroughly how constraining MHD flow influences stationary vortex patterns, (iii) to explain the driving force for the recirculation, (iv) to find the three-dimensional characteristics of the flow, and (v) to clarify whether a two-dimensional flow contains the observed stationary vortex patterns. It will be demonstrated that the decisive parameter for the constrained

MHD flow is the strength of the recirculation between magnetic poles given by the ratio $N/N_{c,m}$, where $N_{c,m}$ is a critical value of the interaction parameter for inducing magnetic vortices in the given magnetic field configuration. Moreover, several successful comparisons with available experimental data will be given for the intensity of the magnetic field, and for a maximal stationary reverse flow inside the magnetic obstacle. It will be shown that the magnetic vortices first appear due to the reverse electromotive force which is induced in order to balance the reverse electrostatic field inside the magnetic obstacle. Also, we will discuss a three-dimensional versus two-dimensional numerical approach and show that the vortices found have a three-dimensional helical structure, while in a two-dimensional model, for the given range of parameters, these vortices are not fixed by the magnetic field and generate vortex shedding.

The subject of the present paper has a close connection to questions of the stability of MHD flows; however, we have not included a full bifurcation analysis of new stationary flow patterns. The paper sheds light on the physical factors that determine the occurrence of stationary recirculation, i.e. the spanwise inhomogeneity of the magnetic field and the necessity of a three-dimensional geometry. We consider the bifurcation and stability analysis as a further step, which – from the practical point of view – involves additional programming work on our code to allow the computation of Jacobi matrices and their eigenvalues in a high-dimensional dynamical system. Therefore, besides others, the following question in particular will remain open: are the topological changes of the flow patterns, which we have observed on changing the system parameters, caused by changes of stability, i.e. bifurcations, or not? This and other open questions deserve further investigation for MHD channel flow in inhomogeneous magnetic field.

The structure of the present paper is as follows. Section 2 presents a sketch of the model, equations and a three-dimensional numerical solver. As an essential part, it describes in §2.2 an analytical method to deal with a magnetic field of arbitrary configuration. Section 3 presents the results of our numerical simulations: stationary flow patterns in the middle plane in §3.1, the stability diagram in §3.3, the mechanism for recirculation in §3.4, the three-dimensional characteristics of vortices in §3.6, as well as a relationship between three-dimensional and two-dimensional numerical methods in §3.7. Finally, the paper ends with conclusions on the observations.

2. Problem definition

2.1. Model, equations, numerical method

A schematic of the model is presented in figure 2: a conducting fluid flows in a rectangular duct of dimensions Length \times Width \times Height = $2L_x \times 2L_y \times 2H$ (the half-length of the duct is shown); the x -axis corresponds to the main direction of the flow. Top, bottom and sidewalls of the duct are no slip and electrically insulating. The magnets of horizontal dimensions Width \times Length = $2M_y \times 2M_x$ are assembled symmetrically on the top and bottom walls, where $2h$ is the distance between north and south poles. The centre of the magnetic gap is the centre of the coordinate system. The constraint factor $\kappa = M_y/L_y$ defines the spanwise distribution of the magnetic field; κ is the geometric parameter varied in the present simulations. Below, we will refer to the case of $\kappa = 0.02$ as a magnetic blade, $\kappa = 0.4$ as a middle magnet, and $\kappa = 1.0$ as a broad magnet.

Unless otherwise specified, throughout the paper the following geometric parameters have been taken: $L_x = 25$, $L_y = 5$, $H = 1$, $h = 1.5$, $M_x = 1.5$, $0.02 \leq \kappa \leq 1$. Reynolds

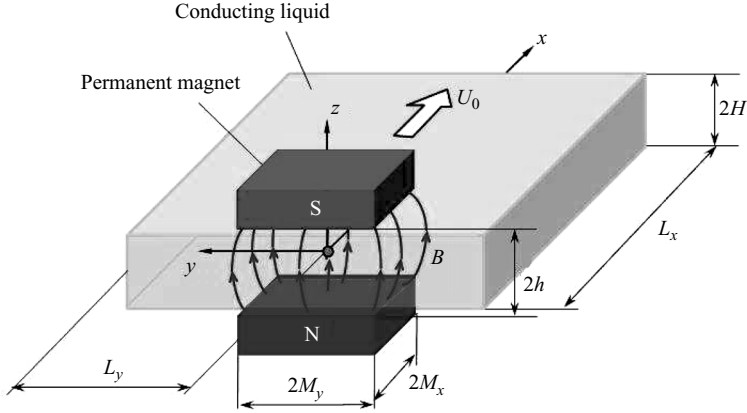


FIGURE 2. Sketch of the model. Throughout the paper the constraint factor $\kappa = M_y/L_y$ is used, where M_y and L_y are half-width of the magnet and duct, correspondingly.

number, Re , and interaction parameter, N , are defined with the half-height of the duct H , the mean flow rate u_0 , and the magnetic field intensity B_0 taken at the centre of the magnetic gap, $x = y = z = 0$.

The governing equations for electrically conducting and incompressible fluid are derived from the Navier–Stokes equation coupled with the Maxwell equations for a moving medium and Ohm's law. We apply the quasi-static (inductionless) approximation where it is assumed that an induced magnetic field is infinitely small in comparison to the external magnetic field, see e.g. Roberts (1967), and is therefore neglected when calculating the Lorentz force, but it is not neglected when finding the electric current density \mathbf{j} . The resulting equations in dimensionless form are

$$\frac{\partial \mathbf{u}}{\partial t} + (\mathbf{u} \cdot \nabla) \mathbf{u} = -\nabla p + \frac{1}{Re} \Delta \mathbf{u} + N(\mathbf{j} \times \mathbf{B}), \quad \nabla \cdot \mathbf{u} = 0, \quad (2.1)$$

$$\mathbf{j} = -\nabla \phi + \mathbf{u} \times \mathbf{B}, \quad \nabla \cdot \mathbf{j} = 0, \quad (2.2)$$

where \mathbf{u} denotes velocity field, \mathbf{B} is an external magnetic field, \mathbf{j} is electric current density, p is pressure, ϕ is electric potential. The interaction parameter N and Reynolds number Re , $N = Ha^2/Re$, are linked by means of the Hartmann number Ha : $Ha = HB_0(\sigma/\rho\nu)^{1/2}$. The Hartmann number determines the thickness of Hartmann boundary layers; $\delta/H \sim Ha^{-1}$; for the flow under a constant magnetic field. For a given conducting fluid and geometry of the duct, we vary either the flow rate velocity u_0 , i.e. Re , or the magnetic field intensity B_0 , i.e. Ha . In both cases, N changes.

For given external field \mathbf{B} , the unknowns of the partial differential equations (2.1)–(2.2) are the velocity vector field $\mathbf{u}(x, y, z)$, and two scalar fields: pressure $p(x, y, z)$ and electric potential $\phi(x, y, z)$. For no-slip and insulating walls, the boundary conditions are $u|_r = 0$, $\partial\phi/\partial\mathbf{n}|_r = 0$, where \mathbf{n} is the normal vector to a surface Γ . The outlet of the duct was treated as a force free (straight-out) boundary for the velocity. The electric potential at the inlet and outlet boundaries was taken to be equal to zero because the inlet and outlet are sufficiently far from the magnetic field. The stationary laminar profile of an infinite rectangular duct known analytically in the form of a series expansion was used as the inlet velocity profile. Because we are interested in a stationary solution, the initial conditions play no role (except for the speed of convergence).

The three-dimensional numerical solver has been described in detail in Votyakov & Zienicke (2007). It was developed from a free hydrodynamic solver created originally in the research group of Professor Dr. M. Griebel (Griebel, Dornseifer & Neunhoffer 1995). The solver employs the Chorin-type projection algorithm and finite differences on an inhomogeneous staggered regular grid. Time integration is by the explicit Adams–Bashforth method that has second-order accuracy. Convective and diffusive terms are implemented by means of the VONOS (variable-order non-oscillatory scheme) scheme. The three-dimensional Poisson equations for pressure and electric potential, arising at each time step, are solved by using the bi-conjugate gradient stabilized method (BiCGStab).

The computational domain, $|x| \leq L_x$, $|y| \leq L_y$, $|z| \leq H$, has been discretized by an inhomogeneous regular three-dimensional grid described in detail in Votyakov & Zienicke (2007). To verify that the inlet and outlet boundaries have no influence on the presented results, we have carried out several simulations with double the number of grid points in the x -direction and found no differences. Moreover, we have also varied the inhomogeneous grid resolution both in the y - and z -direction to ensure that the Hartmann and sidewall layers are properly resolved.

2.2. Fast analytical method for a proper magnetic field

The electrodynamics imposes that an external magnetic field must be divergence- and curl-free. Although authors of previous works realized this, to define their fields they used simple mathematical functions which did not satisfy divergence- and/or curl-free requirements, see e.g. Sterl (1990), Alboussiere (2004). This could be explained by many reasons, e.g. by the complexity of a real field or the insignificance of effects appearing due to an inaccuracy of the field definition. Therefore, there appear to be insufficient correct and yet simple methods to define an external magnetic field of arbitrary configuration. To fill this gap we explain below a simple physical approach which can be easily extended and implemented to three-dimensional numerical models.

We assume that a magnet is composed of perfectly aligned pointwise magnetic dipoles having the same magnetic moment. This assumption is well posed for modern manufactured permanent magnets, as follows from the final comparison between calculated and experimentally measured magnetic fields. Take z as the direction of the unit magnetic dipole $\mathbf{m} = (0, 0, 1)$; then, a partial magnetic field at point $\mathbf{r} = (x, y, z)$ from a dipole located at point $\mathbf{r}' = (x', y', z')$ can be presented as, see e.g. Jackson (1999),

$$\begin{aligned} \mathbf{B}'(\mathbf{r}, \mathbf{r}') &= \nabla \times \left[\mathbf{m} \times \frac{\mathbf{R}}{R^3} \right] = \nabla \times \left[-\mathbf{m} \times \left(\nabla \frac{1}{R} \right) \right] \\ &= \nabla \times \left[\nabla \times \left(\frac{\mathbf{m}}{R} \right) - \frac{1}{R} \nabla \times \mathbf{m} \right] = \nabla \left[\nabla \cdot \frac{\mathbf{m}}{R} \right] = \nabla \frac{\partial}{\partial z} \frac{1}{|\mathbf{r} - \mathbf{r}'|}. \end{aligned} \quad (2.3)$$

where $\mathbf{R} = \mathbf{r} - \mathbf{r}'$ and $R = |\mathbf{r} - \mathbf{r}'|$. Here we have used $\mathbf{R}/R^3 = -\nabla(1/R)$ along with few vector identities and omitted the constant $\mu_0/(4\pi)$. Then, the total field from a magnet occupying a space Ω follows as

$$\mathbf{B}(\mathbf{r}) = \int_{\Omega} \mathbf{B}'(\mathbf{r}, \mathbf{r}') d\mathbf{r}' = \nabla \frac{\partial}{\partial z} \Phi(\mathbf{r}), \quad \Phi(\mathbf{r}) = \int_{\Omega} \frac{d\mathbf{r}'}{|\mathbf{r} - \mathbf{r}'|}. \quad (2.4)$$

The last integral can be computed analytically in some cases as we show below. For an arbitrary Ω , the integration can be performed only numerically and then be once tabulated in a three-dimensional array. This three-dimensional array can be put into a numerical solver where a finite differentiation is applied to compute the

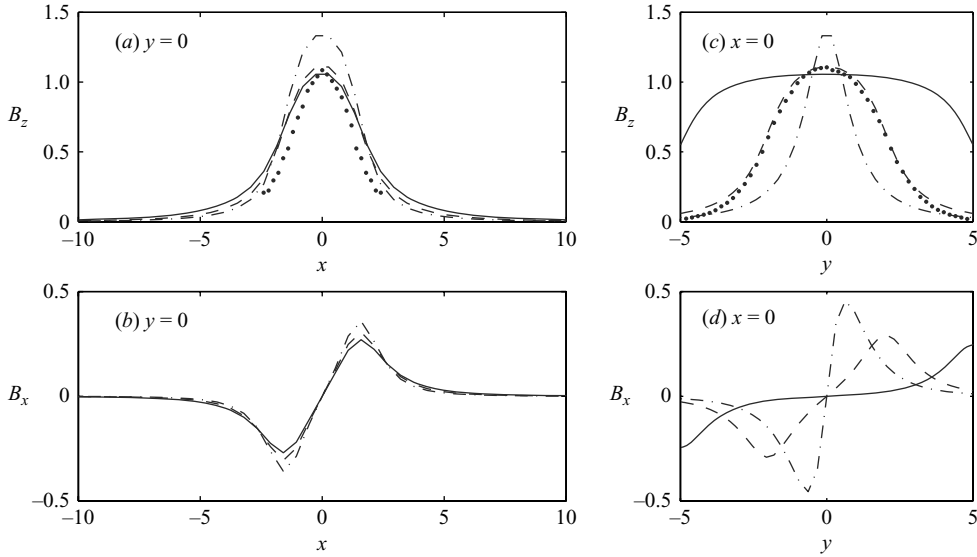


FIGURE 3. Comparison of computed (lines) and experimental (symbols) magnetic field intensities at different $\kappa = M_y/L_y$: $\kappa = 0.02$ (dot-dashed), 0.4 (dashed and symbols) and 1.0 (solid), and $z = -0.7$: (a) B_z component along x , $y=0$, (b) B_x component along x , $y=0$, (c) B_z component along y , $x=0$, (d) B_x component along y , $x=0$.

external magnetic field. Another way is to differentiate analytically $1/|\mathbf{r} - \mathbf{r}'|$ and then calculate numerically three integrals for each magnetic field component.

When the limits of the integration imposed by Ω are independent of each other, then the problem has an analytical solution by means of the indefinite integrals given in the Appendix.

As shown in figure 2, the magnetic dipoles are located in the region $\Omega = \{|x'| \leq M_x, |y'| \leq M_y, h \leq |z'| \leq \infty\}$, where $2h$ is the distance between the north and south magnetic poles. In the present paper, the condition $|z'| \geq h$ is assumed because the magnets used in the experiments are assembled onto a soft-iron yoke that closes magnetic field lines, i.e. the dipoles are effectively located from h to infinity. By taking the corresponding derivatives of indefinite integrals given in the Appendix, and after a few algebraic calculations one obtains

$$B_x(x, y, z) = \frac{1}{B_0} \sum_{k=\pm 1} \sum_{j=\pm 1} \sum_{i=\pm 1} (ijk) \operatorname{arctanh} \left[\frac{y - jM_y}{r(i, j, k)} \right], \quad (2.5)$$

$$B_y(x, y, z) = \frac{1}{B_0} \sum_{k=\pm 1} \sum_{j=\pm 1} \sum_{i=\pm 1} (ijk) \operatorname{arctanh} \left[\frac{x - iM_x}{r(i, j, k)} \right], \quad (2.6)$$

$$B_z(x, y, z) = -\frac{1}{B_0} \sum_{k=\pm 1} \sum_{j=\pm 1} \sum_{i=\pm 1} (ijk) \operatorname{arctan} \left[\frac{(x - iM_x)(y - jM_y)}{(z - kh)r(i, j, k)} \right], \quad (2.7)$$

where $r(i, j, k) = [(x - iM_x)^2 + (y - jM_y)^2 + (z - kh)^2]^{1/2}$, and B_0 is selected in such a way that $B_z(0, 0, 0) = 1$. Three-fold summation with the sign-alternating factor (ijk) reflects the fact that these equations are obtained by integrating according to (2.4).

Figure 3 shows cuts of magnetic field intensities computed with equations (2.5)–(2.7) for different κ . Also, some experimental data (symbols) are presented for $\kappa = 0.4$.

There is a good agreement between experimental and analytical results. Moreover, one can see that the constraint factor κ mainly affects the spanwise distribution of magnetic field, whereas the streamwise distribution changes only slightly. This is expected, because the length M_x of the magnet is fixed, while the width $M_y = \kappa L_y$ is varied. Note that even for the broad magnet ($\kappa = 1.0$) there is still a decline of B_z near sidewalls, figure 3(c).

Contour lines of the B_z component in the middle plane ($z=0$) at different κ are also shown in figure 4(a–c).

Thus, we have demonstrated a self-consistent analytic approach to define arbitrary magnetic field configurations. It guarantees the divergence- and curl-free requirements of $\mathbf{B}(r)$ and has a link with a clear physical model.

3. Results and discussion

3.1. Stationary flow patterns in the middle plane

In §3.1 we discuss characteristic stationary flow patterns which have been extracted from three-dimensional numerical results. Three-dimensionality of the simulations is of importance to make these patterns stable, as we shall show later in §3.7.

3.1.1. Streamlines for different constraintment κ

In our opinion the most striking effect of spanwise heterogeneity of the external magnetic field is shown in figure 4, where flow streamlines in the middle plane, figure 4(d–f), are shown at the same flow parameters, $N = 36$ and $Re = 196$. To get an impression of the magnetic field configurations, the corresponding B_z contour lines are shown in figure 4(a–c). Depending on the constraintment factor κ , one observes the following stationary flow patterns: a vortex dipole for the magnetic blade ($\kappa = 0.02$), figure 4(a, d); the stable six-vortex ensemble for the middle magnet ($\kappa = 0.40$), figure 4(b, e); and no vortex motion for the broad magnet ($\kappa = 1.0$), figure 4(c, f). The projection of the magnetic pole onto the middle plane is shown by the bold solid line.

Let us qualitatively explain these flow patterns. The case of the magnetic blade, figure 4(a, d), might be roughly understood by considering the limiting case of a Lorentz force which is pointwise in the spanwise direction. (By its definition, $\mathbf{F}_L = \mathbf{j} \times \mathbf{B}$, the Lorentz force is a volume force; however, if the distribution of heterogeneous magnetic field \mathbf{B} is very sharp in space, the Lorentz force distribution is also very sharp.) As is known, see e.g. Voropayev & Afanasyev (1994), such an instant retarding force generates vorticity which results in two counter-rotating vortices, a vortex dipole. Then, the induced vortices are advected and diffused downwards from the source of the force. In the case of MHD flow, these two vortices are fixed by a sideways gradient of the magnetic field, so they stay in place. We should note that a similar recirculation has been obtained numerically earlier by Gelfgat *et al.* (1978), and recently by Cuevas *et al.* (2006b) for a creeping flow.

The case of the middle magnet, figure 4(b, e), is explained briefly in Votyakov *et al.* (2007) by means of a mutual interaction of Lorentz and inertial forces. The first pair – inner magnetic vortices – is an inheritor of the vortex dipole as in figure 4(d); the third pair – attached vortices – is of the same nature as recirculation past a solid body, figure 1(a), while the intermediate pair – connecting vortices – appears to make the coherent rotation of the magnetic and attached vortices possible, figures 1(b), 4(e). It is clear why attached (hence, connecting) vortices are not induced in the case of the magnetic blade: it has a streamlined shape, so there is no stagnation region. This

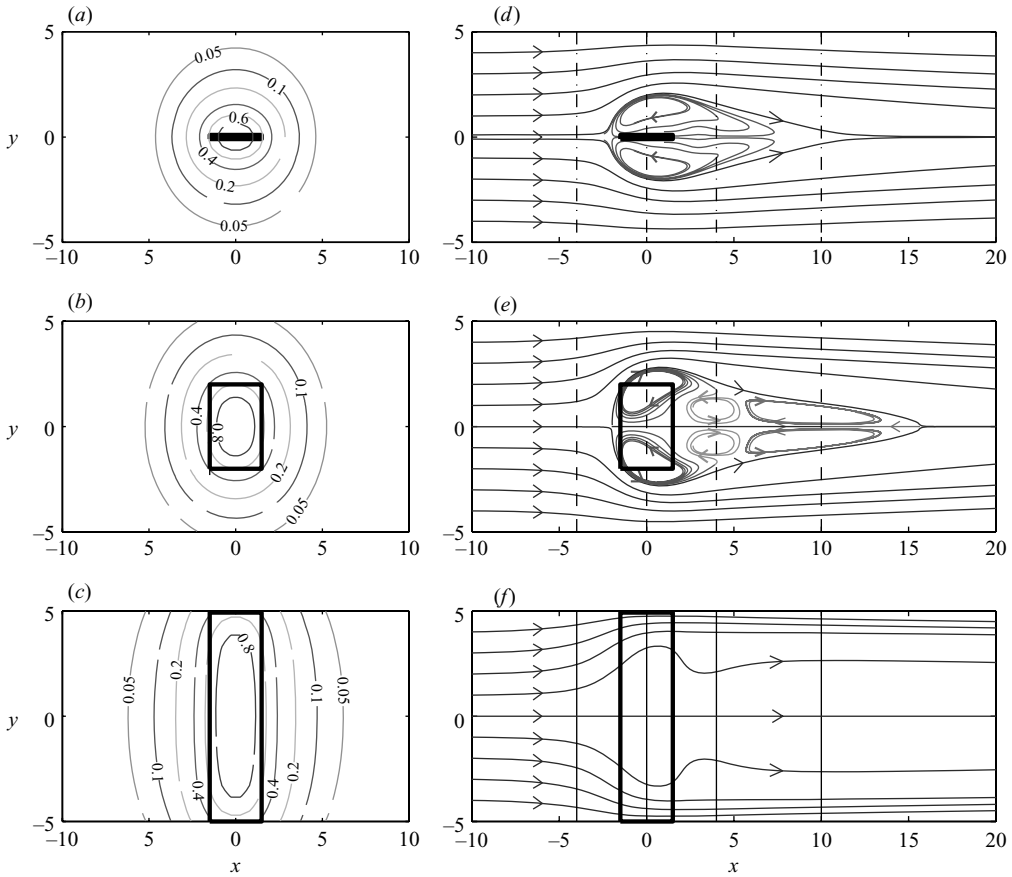


FIGURE 4. (a–c) Contour lines of the transverse magnetic field component and (d–f) flow streamlines in the middle plane ($z=0$) at $N=36$, $Re=196$ and (a, d) $\kappa=0.02$, (b, e) 0.4 , and (c, f) 1.0 . Magnetic pole is shown by bold lines. Dot-dashed (d), dashed (e) and solid (f) vertical cuts denote the location of velocity profiles of figure 5.

is in full analogy with the flow around a solid body where the appearance of the stagnation region is strongly influenced by the extent of streamlining.

Finally, the case of the broad magnet, figure 4(c, f), shows no recirculation at given parameters, because the flow pattern is now influenced mainly by streamwise inward and outward gradients of the magnetic field. As is known, see e.g. Shercliff (1962), Kit *et al.* (1970), Sterl (1990), the streamwise gradients and sidewalls of the duct are together responsible for an M-shaped profile of the streamwise velocity in the spanwise direction. The M-shaped profile can also develop a stagnation region in the middle of the duct at high interaction parameter N ; however, no recirculation has been discovered until now. Moreover, as we shall prove in §3.4, no recirculation is possible if an external magnetic field is perfectly spanwise uniform. The present case of the broad magnet shows a slight decrease of B_z towards sidewalls, see figure 3(c, solid line). In figure 4(c), however, this decrease is not enough to develop magnetic vortices at the given interaction parameter $N=36$. We will see later that the critical interaction parameter $N_{c,m}$ which is needed to induce recirculation under the broad ($\kappa=1.0$) magnetic gap is more than 100.

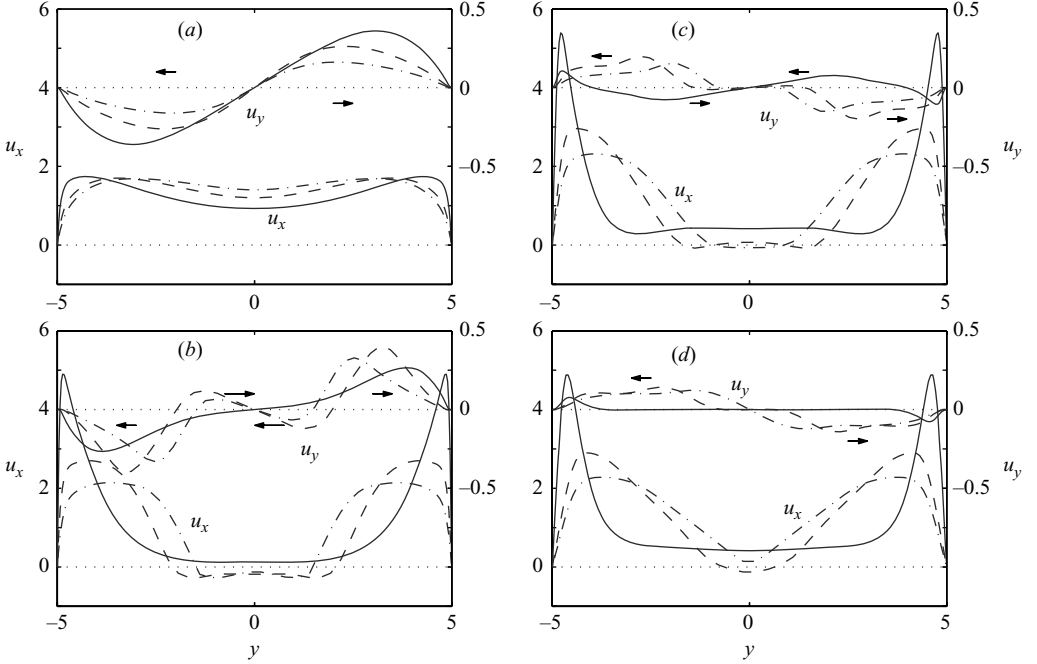


FIGURE 5. Streamwise (u_x , three lower curves, left y-axis) and spanwise (u_y , three upper curves, right y-axis) velocities along the spanwise cuts shown in figure 4(d–f). Middle plane, $z=0$, and (a) $x=-4$, (b) $x=-2$, (c) $x=2$, (d) $x=4$. Constraint factor $\kappa=0.02$ (dot-dashed), $\kappa=0.40$ (dashed), and $\kappa=1.0$ (solid), $N=36$, $Re=196$. Arrows show directions of spanwise redistribution of the flow.

3.1.2. Velocity profiles at different κ and the same N and Re

Figure 5 shows quantitative data on stream- and spanwise velocity along different spanwise cuts. Different line styles correspond to the different κ . Arrows in figure 5 show directions of spanwise redistribution of the flow.

The largest braking Lorentz force, $\mathbf{F}_L = \mathbf{j} \times \mathbf{B}$, is generated at the front of a magnetic obstacle where induced electric currents \mathbf{j} are maximum and the magnetic field \mathbf{B} is strong. This results in the deformation of the incoming flow on the obstacle by $x=-4$, figure 5(a). The deformation consists of an inhomogeneous M-shaped profile of streamwise velocity u_x and the appearance of a spanwise flow, i.e. u_y , from the centre to the sidewalls, as shown by arrows in figure 5(a).

Despite the order of magnitude difference in spanwise widths of magnets for $\kappa=0.02$ (dot-dashed) and $\kappa=0.4$ (dashed), their ranges of reverse velocity ($u_x \leq 0$, figure 5(b)) along the y -axis differ only by a factor 1.5 in the area of magnetic vortices. Positive streamwise velocities of the vortices are smoothly transformed into velocities of the external flow. Thus, for the wide range of κ , the spanwise diameter of a single magnetic vortex remains nearly constant provided the vortex is not influenced by a sidewall. This is a manifestation of the fact that a decisive factor for the vortex is the width of the spanwise decline of a magnetic field rather than the width of the magnet.

By forming magnetic vortices, the M-shaped profile of streamwise velocity u_x develops a negative value in the centre, while the spanwise velocity u_y changes its sign twice. There is a redistribution of the flow from the vortex inner side to the centreline ($y=0$), and from the external side of the vortex to the corresponding sidewall ($y=L_y$).

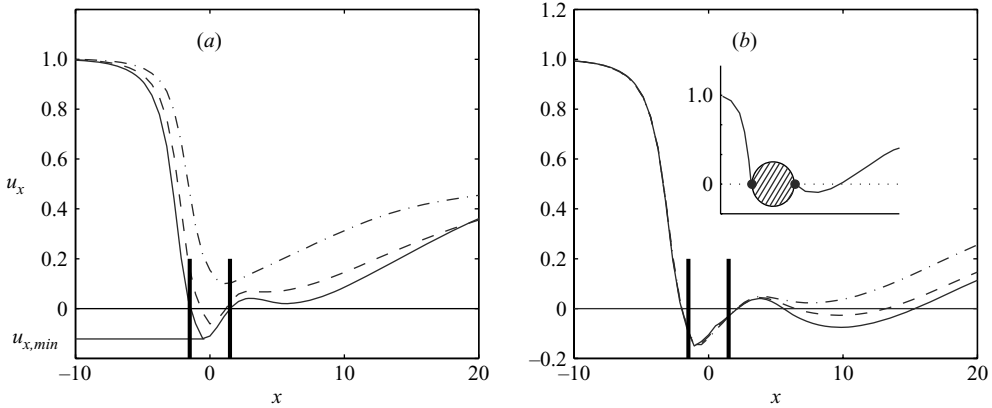


FIGURE 6. Variation of streamwise velocity varied along the centreline $y = z = 0$ for the middle magnet ($\kappa = 0.4$): (a) effect of N at fixed $Re = 100$; and (b) effect of Re at fixed $N = 36$. For (a): $N = 4$ (dot-dashed), 9 (dashed), and 16 (solid lines); for (b): $Re = 100$ (dot-dashed), 144 (dashed), and 196 (solid lines). Vertical bold lines show edges of the magnetic gap, $M_x = 1.5$. Inset in (b) is a centreline velocity profile for a flow around a circular cylinder with attached vortices. The streamwise velocity is normalized with the centreline velocity of unretarded flow.

On the other hand there are distinct zones past the magnetic vortices where a spanwise redistribution is absent ($u_y = 0$), see $|y| \leq 0.8$ for the magnetic blade ($\kappa = 0.02$, dot-dashed) and $|y| \leq 1.5$ for the middle magnet (dashed), figure 5(c). Also, a zone of $u_y = 0$ is observed behind attached vortices, $|y| \leq 1$, figure 5(d), $\kappa = 0.4$.

The streamwise component of the velocity shows small changes with increasing x , cf. u_x in figure 5(b–d), except for a single peculiarity. For the case of a broad magnet ($\kappa = 1$, solid lines), as x increases, the maximum of u_x is shifted from the sidewalls to the centre due to diffusion of vorticity. At the same time, the u_y component changes its sign in the region near the sidewalls.

3.2. Centreline profiles

In this Section, taking as an example the middle magnet, $\kappa = 0.4$, we show what forces are needed to induce vortices inside and past a magnetic obstacle. To reach this goal we shall analyse streamwise velocities along the centreline of the duct ($y = z = 0$), i.e. centreline profiles.

The main difference between a magnetic obstacle and a solid body is the permeability of the obstacle depending on the retarding Lorentz force, $\mathbf{F}_L = \mathbf{j} \times \mathbf{B}$. This braking force is largest in the centre of the magnetic obstacle, where the magnetic field \mathbf{B} reaches the highest intensity. The characteristic measure of the Lorentz force with respect to inertia is given by the interaction parameter N : the higher N , the stronger is \mathbf{F}_L and the less penetrable is the space under the magnets. Figure 6(a) illustrates this behaviour: the dot-dashed line ($N = 4$) shows that the streamwise velocity is suppressed on approaching the magnet; however the braking force for the given N is not strong enough to reverse the flow. The reversal happens at higher N , see dashed ($N = 9$) and solid ($N = 16$) lines being negative inside the obstacle. The lowest velocity is marked in figure 6(a) by $u_{x,min}$; it becomes zero at a critical value $N_{c,m}$, and at $N \geq N_{c,m}$ one observes a recirculation – two inner magnetic vortices as shown in figure 4(d, e). As the name suggests, these vortices belong completely to the MHD flow, and have nothing in common with a hydrodynamical flow around a cylinder. Rather, these vortices are similar to those appearing under the action of

a point braking force, see e.g. Afanasyev (2006). The concrete mechanism leading to the magnetic vortices is presented in §3.4.

Now, we consider the behaviour of centreline curves at fixed N and varying Re , figure 6(b) and apply the analogy with ordinary hydrodynamics. Let us recall that the flow around a solid cylinder shows a stagnant region with two attached vortices when Re is slightly higher than a critical value. The typical centreline for this case is shown in the inset of figure 6(b). The same situation can happen for the magnetic obstacle by increasing Re : the centreline curves past the magnetic gap become negative again as shown in figure 6(b). In fact, attached vortices are induced past the magnetic obstacle, see figure 4(e, third pair of vortices) analogous to those past a real solid body.

Note that the first minimum in a centreline profile is almost unperturbed when Re increases at fixed N , figure 6(b), and this is more strong evidence that the vortices inside and past the magnetic obstacle are of different physical origin. Since the interaction parameter is given as $N = Ha^2/Re$, the magnetic vortices are enhanced by decreasing the flow rate (i.e. Re). On the other hand, as follows from figure 6(b), the attached vortices manifest themselves by increasing the flow rate provided that the intensity of the magnetic field (i.e. Ha) as well as a spanwise magnetic field gradient have already enforced a reverse flow inside the magnetic obstacle. In other words, there is a qualitative distinction between magnetic and attached vortices: the former arise when Re decreases, and the latter arise when Re increases provided Ha is strong.

It is easy to see in figure 4(e) that magnetic and attached vortices are co-rotating in a direction determined by the main flow movement. The only difference is the driving torque: this is the Lorentz force for the magnetic vortices, and the inertial force for the attached vortices. Because the MHD and attached vortices are co-rotating, such a motion must be accompanied by a counter-rotation which produces the intermediate pair of connecting vortices, see figure 4(e, second pair of vortices). The connecting vortices correspond to a local maximum on centreline curves, see figure 6(b) behind the magnetic gap.

Thus, N is responsible for the appearance of the magnetic vortices, while Re is responsible for the appearance of the attached vortices. The connecting vortices are necessary for the coherent rotation of the magnetic and attached vortices.

Three decades ago Gelfgat *et al.* attempted to reveal a kind of recirculation due to an external magnetic field by both two-dimensional numerical simulation (Gelfgat *et al.* 1978) and physical experiments (Gelfgat & Olshanskii 1978). They saw a reverse flow numerically, and then designed a special experiment but it did not confirm the recirculation. It follows from our results that the authors of the cited papers had not realized that they had observed and discussed different phenomena in their numerical and experimental works. Their two-dimensional numerical study neglected an inertial term, which corresponds to a creeping flow, and the observed reversal of the flow is just a sign of magnetic vortices. Recently, similar two-dimensional numerical work by Cuevas *et al.* (2006b) showed the same effect in a creeping flow without sidewalls. Thus, the numerical work of Gelfgat precedes Cuevas *et al.* (2006b) by almost thirty years.

The experimental report of Gelfgat & Olshanskii (1978) contains a measured centreline profile (see their figure 7b), which falls behind the magnet, but does not approach negative velocities. In the cited experiment, parameters are $N = 7.5$ and $Re = 3.73 \times 10^5$, so the authors noticed that the observed decreasing velocity is due to inertial effects. Moreover, these experiments were performed for turbulent flow because Re is rather high. To obtain the desired recirculation, the authors needed to decrease the inertial force further by using a lower flow rate. This would have resulted in a

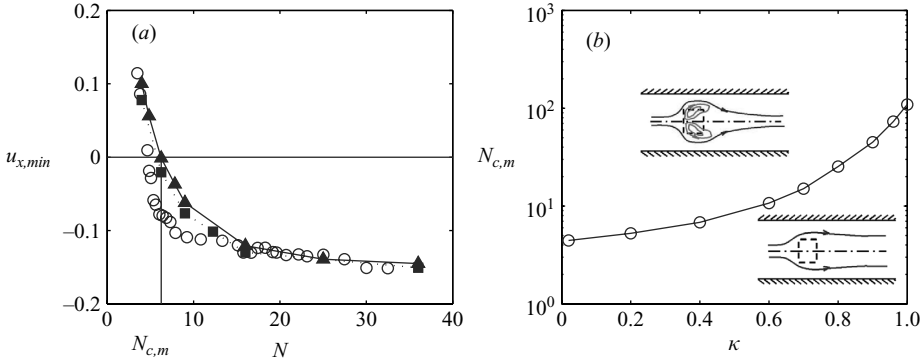


FIGURE 7. (a) Minimum of streamwise velocity on the centrelines curves (see figure 6a) depending on the interaction parameter $N = Ha^2/Re$ obtained in simulations (filled symbols) and in experiments (open circles) for $\kappa = 0.4$ and $Ha = 140$ (experiment), $Re = 196$ (squares) and $Re = 100$ (triangles). (b) The critical interaction parameter $N_{c,m}$ dependence on κ for the appearance of magnetic vortices, three-dimensional simulation, $Re = 100$.

higher N and, by exceeding some threshold, made the turbulent pulsations impossible. Then, the recirculation by the braking Lorentz force might have been revealed via the appearance of magnetic and attached vortices. Unfortunately, experiments with lower Re have not been performed, probably because the proper analysis of centreline curves (see figure 6) was not then available.

3.3. Existence regions of stationary flow patterns in parameter space

A sign of the recirculation enforced by the Lorentz force is the negative value of $u_{x,min}$, see figure 6(a). We have performed a series of three-dimensional simulations for the different interaction parameters N and constraint factors κ . An example of the series for the middle magnet ($\kappa = 0.4$) is shown in figure 7(a). It is accompanied by experimental data which were obtained by Oleg Andreev for the paper by Votyakov *et al.* (2007) but not reported there due to lack of space. Note that the interaction parameter $N = Ha^2/Re$ is changed differently in the experiments and numerics: experimentally by varying the flow rate (i.e. Re) at fixed external magnets (experimental $Ha = 140$), while numerically by keeping Re constant and changing Ha . This is because of (i) experimental difficulties working with a low flow rate in the closed channel, and (ii) numerical problems arising due to boundary layers at high Hartmann numbers. Moreover, a transition to a turbulent regime is another factor that obscures stationary effects in the numerics at high Re .

As one can see in figure 7(a), $u_{x,min}$ is positive at low N , and then falls monotonically to a constant level, showing perfect agreement between experiments and numerics for $N > 15$. This excellent agreement confirms that the flow under magnets depends solely on N and magnetic field configuration rather than Re or inlet profile, provided the external magnetic field is strong enough to suppress inward turbulent fluctuations. The latter condition was satisfied in experiments by Andreev *et al.* (2007). Also, similarity of the electric potential map at equal N and different Re has been recently confirmed by three-dimensional simulations and comparison with experiments, see Votyakov & Zienicke (2007). The slight difference shown in figure 7(a) at $N < 15$ is explained by the fact that the variation of N has been defined differently in experiments and numerics, as explained above.

The dependence of $u_{x,min}$ on N becomes negative at a critical value $N_{c,m}$. This value depends on the constraint factor κ . A series of three-dimensional simulations has been carried out for the range $0.02 \leq \kappa \leq 1$ in the vicinity of $u_{x,min}(N) \approx 0$ and the results are given in figure 7(b), which shows the separation between regions of stable flow without and with magnetic vortices[†]. During this series of simulations we never found a hint that both flow patterns – one with and one without magnetic vortices – coexist for the same pair of parameters, i.e. both solutions are stable, but have different basins of attraction. However, we have checked different initial conditions only for some parameter combinations and did not carry out a systematic search with different initial conditions. Therefore, we cannot conclude that the case of coexistence of two solutions is impossible.

From the separation line of figure 7(b), as we have numerically determined it the following trends are visible: the lower κ , the smaller the influence of sidewalls; the case of $\kappa \rightarrow 0$ corresponds to a free flow. The larger κ , the more uniform is the braking Lorentz force in the spanwise direction. Therefore, in order to induce inner vortices at larger κ it is necessary to apply a larger critical interaction parameter $N_{c,m}$. For the middle magnets, $\kappa \leq 0.5$, the critical value of $N_{c,m}$ is of the same order of magnitude, $N_{c,m} \approx 6$, and for broad magnets, $\kappa \geq 0.8$, it increases up to $N_{c,m} = 109$ at $\kappa = 1$. The latter case has been discussed earlier in figure 4(c, f) for $N = 36$ as an example of a vortex-free flow pattern. We prove in the next Section that any recirculation is impossible if the external magnetic field is perfectly spanwise uniform.

3.4. The mechanism to induce recirculation: vorticity, electric field, drop of pressure

One has to analyse the electric field inside the magnetic obstacle for different κ in order to understand why the appearance of vortex motion is strongly dependent on the spanwise variation of the external magnetic field.

Let us recall that the electric potential, ϕ , is distributed according to the Poisson equation, $\Delta\phi = \nabla \cdot (\mathbf{u} \times \mathbf{B}) = \mathbf{B} \cdot \boldsymbol{\omega}$, where $\boldsymbol{\omega} = \nabla \times \mathbf{u}$ is the vorticity. Note that the projection of $\boldsymbol{\omega}$ on the externally fixed vector \mathbf{B} plays the role of an induced electric charge density which creates the electrostatic field $\mathbf{E} = -\nabla\phi$. It is possible to derive the direction of the field \mathbf{E} from knowledge of positive and negative extrema in the $\mathbf{B} \cdot \boldsymbol{\omega}$ distribution, by roughly assuming that these extrema can be approximated as point charges. As shown in electrostatics, the maximum (minimum) of the right-hand side of the in Poisson equation, i.e. $B_z\omega_z$, creates the minimum (maximum) in the ϕ distribution.

For definiteness we consider the central spanwise cut, $x = z = 0$, where $B_x = B_y = 0$, $B_z \geq 0$, and $\mathbf{B} \cdot \boldsymbol{\omega} = B_z\omega_z \approx -B_z\partial u_x/\partial y$. This cut goes through the centre of the magnetic gap and clearly shows characteristics typical of any spanwise cut. Vorticity ω_z , the product $B_z\omega_z$, and resulting electric potential ϕ along this central spanwise cut are shown in figure 8 for the broad (a) and middle (b) magnet. The magnets are depicted at the top and bottom by filled rectangles.

The behaviour of vorticity, $\omega_z \approx -\partial u_x/\partial y$, can be easily understood from the spanwise deformation of the streamwise velocity, i.e. M-shaped velocity profile,

[†] It is tempting to call figure 7(b) a stability diagram. We do not do this, because – strictly speaking – it is not proven that the change of topology of the flow patterns is caused by a change of stability. We find this assumption highly probable, but we did not compute eigenvalues of the Jacobi matrices for the stable flow patterns to check whether the transition is a bifurcation or not (see also our remark at the end of the introduction). We continue to call $N_{c,m}$ the critical interaction parameter. This has to be understood not in the sense of a change of stability, but instead in the sense of separating stable solutions with different topology.

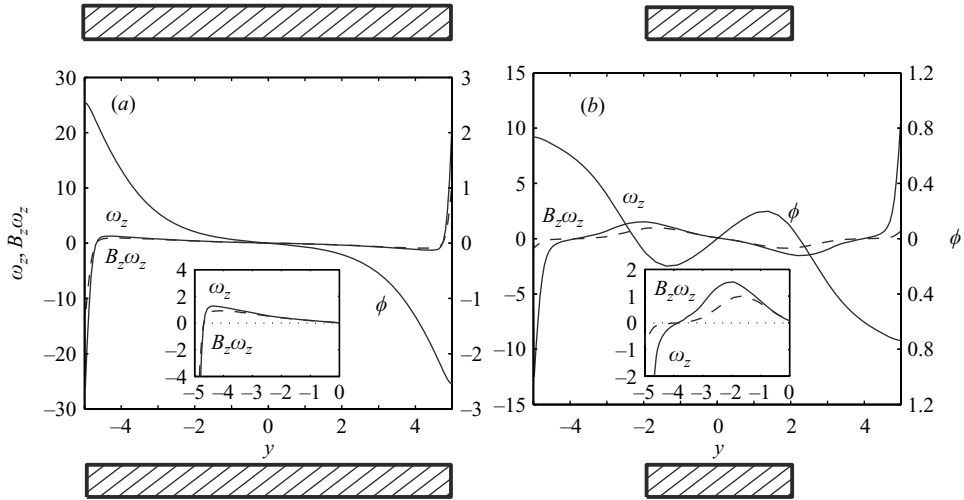


FIGURE 8. Spanwise cuts, $x = z = 0$, of vorticity, ω_z (left axis, solid), magnetic field multiplied by vorticity, $B_z \omega_z$ (left axis, dashed), and electric potential, ϕ (right axis), for (a) $\kappa = 1$ and (b) 0.4 ; $N = 9$, $Re = 100$. Filled rectangles at top and bottom show schematically the magnets.

figure 5(c). Such a profile is characterized by two jets streamlining alongside the magnetic obstacle, and each jet has internal and external slope; hence, the vorticity alternates its sign by passing the velocity maximum of the jet. The steepness of the external side of the jet is significantly higher than that of the internal side, especially for the larger κ because the external slope is next to no-slip sidewalls. Figure 8 shows that the sidewall vorticity, i.e. the external slope vorticity, is larger by an order of magnitude than the vorticity next to the centre, i.e. the internal slope vorticity. To stress this fact, figure 8 shows both global and enlarged (insets) views for ω_z and $B_z \omega_z$.

When the spanwise variation of the magnetic field $B_z(y)$ is weak, e.g. for the broad magnet ($\kappa = 1$) shown in figure 8(a), the product $B_z \omega_z$ reflects completely the quantitative difference in ω_z on the internal and external jet sides. Because the external ω_z is much higher than the internal ω_z , the distribution of ϕ is determined mainly by the vorticity generated on sidewalls rather than by that produced inside the obstacle. Therefore, the negative (positive) external ω_z induces a strong positive (negative) potential on the sidewalls, and $\phi(y)$ drops monotonically along the y -axis, i.e. the spanwise electrostatic field $E_y = -\partial\phi/\partial y$ is always positive and does not change its sign between the sidewalls.

If the magnetic field is perfectly uniform along the y -axis, the electric potential distribution is completely governed by the sidewall vorticity, and the alternating vorticity on the internal slopes of the M-shaped profile does not contribute to $\phi(y)$ even at large interaction parameter N . As a result, the electrostatic field $\mathbf{E} \approx (0, E_y, 0)$ in the region of the magnetic obstacle is always directed opposite to the electromotive force, $\mathbf{u} \times \mathbf{B} \approx (0, -u_x B_z, 0)$. On braking the flow, the streamwise velocity u_x and spanwise field E_y accordingly approach zero by keeping their signs. A stagnant region can develop where streamwise velocity is small but still positive because the electric field is always in the same direction. Therefore, recirculation is impossible.

Let us consider the case when the magnetic field intensity, $B_z(y)$, decreases from the centre to the sidewalls. Here, the high vorticity generated by the sidewalls in

the product $B_z\omega_z$ is suppressed by the low intensity of the magnetic field. This is shown by the middle magnet ($\kappa = 0.4$), figure 8b); the corresponding $B_z(y)$ is shown by dashed lines in figure 3(c). The product $B_z\omega_z$ resembles the $\omega_z(y)$ behaviour inside the magnetic obstacle, since there $B_z(y) \approx \text{const}$, i.e. the internal vorticity is well represented in $B_z\omega_z$. Outside the obstacle, $B_z(y)$ rapidly decreases, so the external vorticity is greatly weakened: as follows from figure 8(b), the dashed $B_z\omega_z$ curve diverges from the solid ω_z curve. The largest difference between ω_z and $B_z\omega_z$ is on the sidewalls where the external vorticity is very high due to no-slip boundary conditions, while $B_z\omega_z$ at $|y| = L_y$ is of the same magnitude because its alternating extrema at $|y| \approx M_y$ correspond with the edges of the magnet. Therefore, the dependence of $\phi(y)$ can be influenced by the internal slopes of the M-shaped profile, which produces extrema on $\phi(y)$ at $|y| \approx M_y$, alternating with the sign of ϕ on sidewalls. These internal extrema on $\phi(y)$ reverse the spanwise electric field, i.e. $E_y = -\partial\phi/\partial y$ becomes negative inside a finite magnetic obstacle.

The reverse spanwise electrical field appearing for a spanwise decaying magnetic field is a necessary but not sufficient condition for the appearance of reverse flow. It is a necessary condition, because otherwise no Lorentz force pointing in the negative x -direction would appear. This becomes clear by looking at equations (2.1) and (2.2) for the Lorentz force and current density: $\mathbf{j} \times \mathbf{B} = -\nabla\phi \times \mathbf{B} - B^2\mathbf{u} + (\mathbf{u} \cdot \mathbf{B})\mathbf{B}$. Considering again the central spanwise cut, $x = z = 0$, where $\mathbf{B} = (0, 0, B_z)$, $\mathbf{u} \approx (u_x, 0, 0)$ and $\mathbf{j} \approx (0, j_y, 0)$, one can write the x -component of the Lorentz force as follows: $(\mathbf{j} \times \mathbf{B})_x \approx j_y B_z = E_y B_z - B_z^2 u_x$. The third term has vanished, and the second term corresponds to a frictional force proportional to the velocity. The only term which can provide a driving force for the reverse flow is the first term, and this only then when E_y is negative, i.e. when a reverse spanwise electrical field exists. However, the existence of a reverse spanwise electrical field is not sufficient to drive reverse flow, because it has to reach a minimal strength. This becomes clear from considering the y -component of Ohm's law for the electrical current density at the central spanwise cut: $j_y = E_y - u_x B_z$. To see this, one needs additional information concerning the global behaviour of the electrical current in our system. The electrical current is organized in two horizontal loops, with a strong negative spanwise current (i.e. $j_y < 0$) directly under the magnet, which divides at the sidewalls into one loop in front of the magnet and the other behind it (see figures 16, 17 and 18 of Votyakov & Zienicke 2007). The sign of j_y does not change when the interaction parameter is increased. When E_y just changes sign at a certain value of N at the start of electric field reversal, $-u_x B_z$ must be negative. This is only possible for (still) positive u_x , and consequently N must be further increased until the reverse spanwise electrical field becomes so strong that it equals j_y . This characterizes the critical $N_{c,m}$, for which the velocity u_x is exactly zero. Let us denote this value of the reverse spanwise electrical field by $E_{y,c}$. A further increase of the interaction parameter makes E_y more strongly negative than j_y with the consequence that u_x must be smaller than zero, which is equivalent to the existence of reverse flow and recirculation. Thus, summing up, the role of the spanwise magnetic field gradient is to suppress the external vorticity and promote the internal vorticity in the product of $\mathbf{B} \cdot \boldsymbol{\omega}$. When on a further increase of the interaction parameter the internal spanwise electrostatic field is reversed more strongly than the critical $E_{y,c}$, the recirculation appears.

Figure 9(a) shows $E_y = -\partial\phi/\partial y$ for the different magnets, taken in the centre of the magnetic gap, $x = y = z = 0$, as a function of the interaction parameter N normalized with the critical value $N_{c,m}$. Taking the appearance of recirculation as the reference flow pattern, the ratio $N/N_{c,m}$ characterizes the strength of recirculation for various

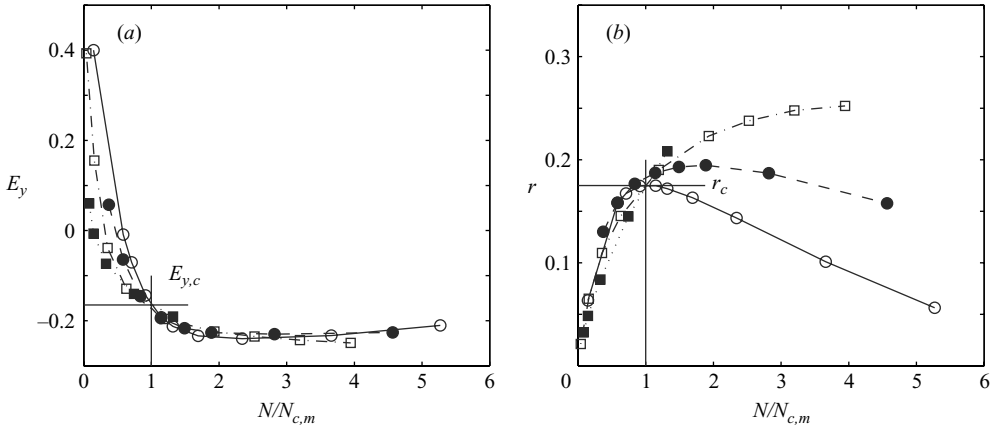


FIGURE 9. The dependence on $N/N_{c,m}$ in the centre of the magnetic obstacle, $x = y = z = 0$ of (a) the spanwise electrostatic field, $E_y = -\partial\phi/\partial y$, and (b) the normalized resistance to the flow, $r = (-\partial p/\partial x)/N_{c,m}$, for various magnetic field configurations, $\kappa = 0.4$ (open circles), 0.6 (filled circles), 0.8 (open squares), 1.0 (filled squares).

κ . One can see that the curves are close to each other when $N/N_{c,m} \gtrsim 1$. Moreover, when $N/N_{c,m} = 1$ one finds that the critical $E_{y,c} \approx -0.17$ is independent of κ . That is, the critical magnitude of the spanwise electrostatic field, $E_{y,c}$, is a universal parameter which is the same for different magnetic field configurations. This is clear because $B_z = 1$ and $j_y = E_{y,c}$ when the recirculation starts, i.e. $u_x = u_y = 0$. So, $E_{y,c}$ is indeed the critical braking Lorentz force because $F_{L,x} = j_y B_z = E_{y,c}$.

Let $r = -(\partial p/\partial x)/N_{c,m}$ at $x = y = z = 0$ be the resistance to the flow inside the magnetic obstacle. At the beginning of recirculation the Navier–Stokes equation is simplified up to $\partial p/\partial x + N_{c,m} E_{y,c} = 0$, so $r_c = -E_{y,c}$. The behaviour of r as a function of $N/N_{c,m}$ for various κ is shown in figure 9(b). One can see that a change of the flow regime is accompanied by a change of the slope in the resistance of $r(N/N_{c,m})$. For those κ where the sidewall influence is insignificant, the appearance of recirculation at $N/N_{c,m} \gtrsim 1$ results in a drop in the resistance despite the fact that N increases.

The second effect of a drop in the resistance due to magnetic recirculation has the same explanation as the ‘drag crisis’ well known in hydrodynamics. It appears in the wake of a circular cylinder when the boundary layer on the cylinder surface undergoes a transition from the laminar to turbulent mode. It causes a substantial reduction in the drag force analogous to that in the wake of the magnetic obstacle.

3.5. Similarity of MHD flows inside the magnetic obstacle

As follows from (2.1) the viscous force $\Delta \mathbf{u}$ is scaled by Reynolds number Re ; therefore at high Re and far from the walls it plays a minor role. As a result the flow must be governed by the interaction parameter N defining the ratio between magnetic and inertial forces. This peculiarity was noted in Votyakov & Zienicke (2007) by comparing experimental and numerical electric potential distributions found at different Re and similar N .

In the present paper, figure 10 demonstrates the same behaviour for the broad (curves 1 and 3) and middle (curves 2) magnets. Solid and dashed curves 1, 2 have the same N but $Re = 100$ for solid and $Re = 400$ for dashed lines.

It is expected from the discussion of figure 9 that the results given in figure 10 would be similar even for different constraint factors κ and interaction parameters N

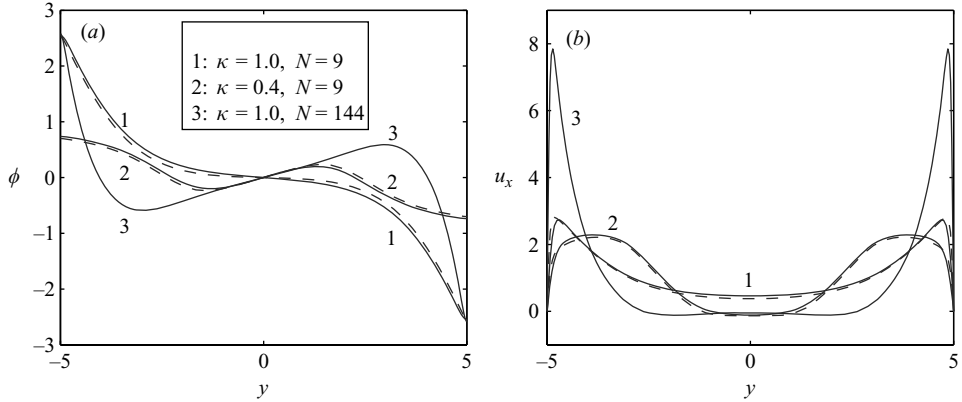


FIGURE 10. Spanwise dependence ($x=z=0$) of (a) electric potential and (b) streamwise velocity for the broad ($\kappa=1.0$, $N_{c,m}=109$, solid and dashed curves 1, 3) and middle ($\kappa=0.4$, $N_{c,m}=6.8$, solid and dashed curves 2) magnetic obstacle. $N=9$ (curves 1, 2) and 144 (curves 3), $Re=100$ (solid) and 400 (dashed lines). Notice that for the curves 2 and 3 the constraint factors κ are different, while the relations $N/N_{c,m} \approx 1.32$ are equal.

provided the corresponding ratios $N/N_{c,m}$ are equal. Curve 2 for the middle magnet is plotted for $N=9$, i.e. $N/N_{c,m}(\kappa=0.4)=9/6.8=1.32$ and curve 3 for the broad magnet for $N=144$, i.e. $N/N_{c,m}(\kappa=1.0)=144/109=1.32$. One can see that in the central part $|y| \lesssim 2$, being approximately the spanwise dimension of the smaller magnet ($M_y=0.4 \times 5=2$), both electric potential (a) and streamwise velocity (b) are also close to each other, cf. curves 2 and 3.

3.6. Three-dimensional characteristics of the flow

Figure 11 shows different three-dimensional space perspective views of chosen streamlines inside the six-fold vortex pattern for the middle magnet ($\kappa=0.4$), $N=16$, and $Re=196$. For easy visualization, plot (a) shows the XY projection of all vortices, i.e. magnetic, connecting, and attached, while other plots present only part of the recirculation. Plot (b) shows the XZ projection for magnetic and attached vortices, plots (c, d) are YZ projections of the magnetic and attached vortices, respectively.

The following three-dimensional features are observed in figure 11: (i) a helical motion inside every vortex; (ii) the axes of rotation of the magnetic vortices are parallel to the lines of external magnetic field; (iii) the two magnetic vortices are closely adjoined to each other and taken together they form a barrel with an extended central part and located mainly between the magnetic poles; (iv) two helices of attached vortices are not adjoined and are arched along the x -direction.

Additionally, figure 12 presents flow streamlines constructed from the u_y and u_z components of velocity field for a few characteristic vertical slices: in front of the magnet ($x=-4$, plot a), and vertical cuts of magnetic ($x=0$, plot b), connecting ($x=4$, plot c) and attached ($x=8$, plot d) vortices. These (u_y, u_z) streamlines are not lines of moving fluid particles in the vertical slices, because the particles have also an u_x velocity component. Instead, these streamlines are intended to show ascending and descending paths of fluid particles in vertical slices as projection.

At $x=-4$, figure 12(a), one observes the braking effect of the Lorentz force making the flow streamlines diverge from the central point $y=z=0$, where the greatest change of $\partial u_x / \partial x = -(\partial u_y / \partial y + \partial u_z / \partial z)$ occurs. Because the u_x component is not involved in the plot, this effect appears to be the source of the flow. Also there is motion in the

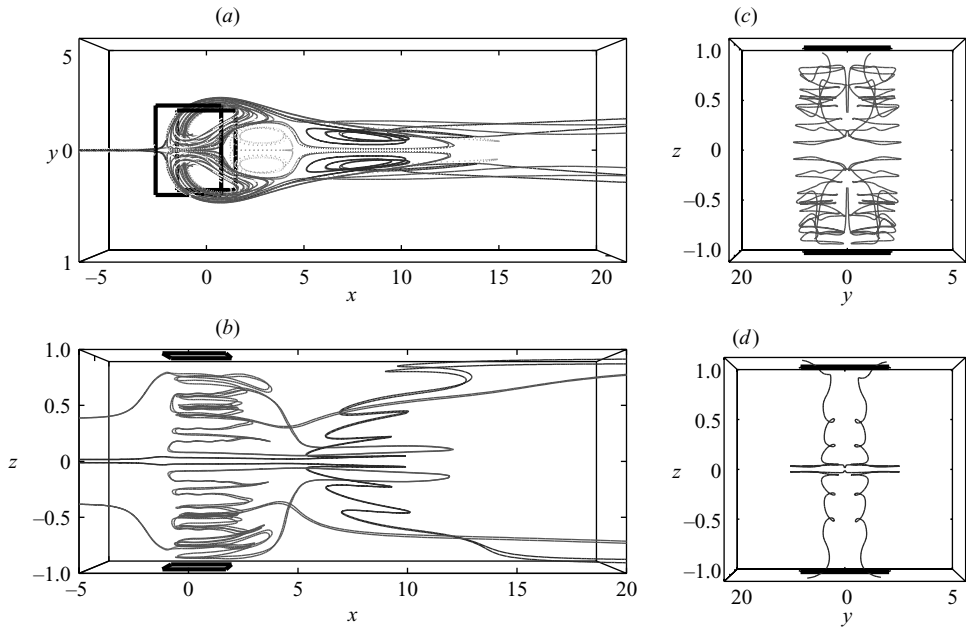


FIGURE 11. Perspective projection of three-dimensional vortex disposition for middle magnet and $N = 16$, $Re = 196$: (a) XY view, magnetic, connecting and attached vortices, (b) XZ view, magnetic and attached vortices, (c) YZ view, magnetic vortices, (d) YZ view, attached vortices. The fluid motion inside the vortices is visualized by properly chosen streamlines.

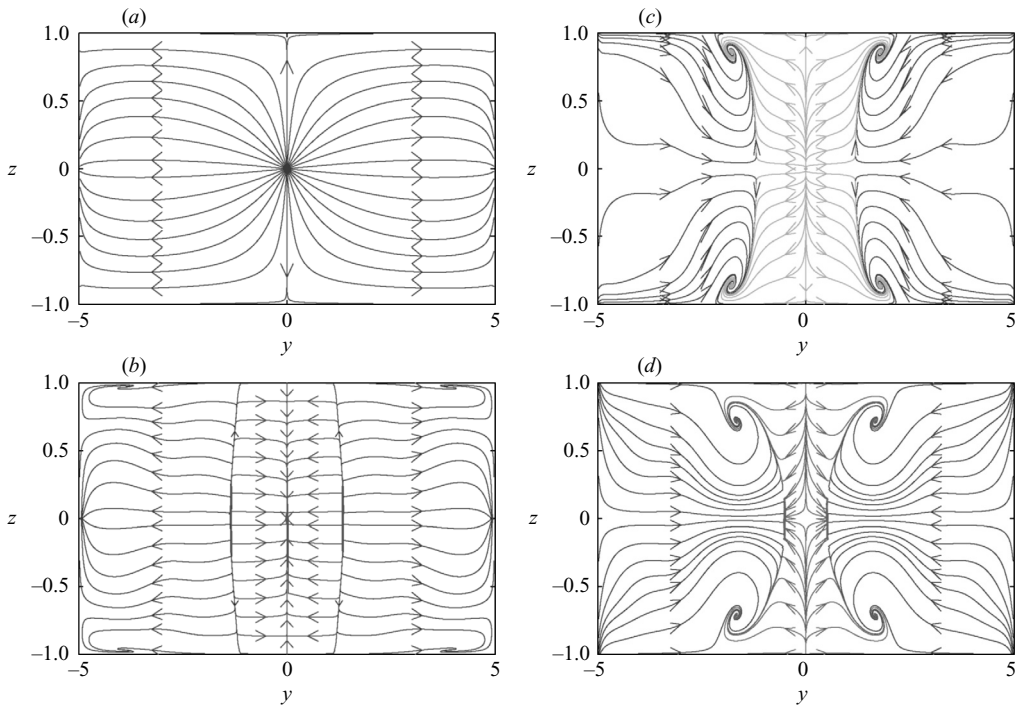


FIGURE 12. Flow streamlines constructed from u_y, u_z velocity components in vertical slices (a) $x = -4$, (b) 0, (c) 4, and (d) 8; $N = 16$, $Re = 196$.

z -direction caused by a tendency to form Hartmann layers, see Votyakov & Zienicke (2007).

At $x=0$, figure 12(*b*), one first notices the abrupt change of the motion in the y -direction at $|y| \approx 2$. This helps us to see the vertical borders of the magnetic vortices where the u_y reverse its sign. Moreover, the barrel shape of the magnetic vortex dipole can be clearly seen. Directions of arrows on the flow streamlines demonstrate a drift of the flow from top/bottom walls towards the centre inside the magnetic vortices, and a drift in the opposite direction outside them. Such a drift is a reflection of helical motion which can be seen in perspective in figure 11.

Similar to figure 12(*b*), sharp boundaries between the main flow and connecting ($x=4$, figure 12*c*) and attached ($x=8$, figure 12*d*) vortices are observed. One also observes a remarkable vertical drift to and from the top and bottom walls depending on the direction of horizontal rotation. The vertical drift at $x=4$ and $x=8$ is more pronounced than that at $x=0$ because the magnetic field has a much larger intensity in the case of $x=0$. The new phenomena compared to figure 12(*b*) are the swirls in the corners of the duct shown in figure 12(*c, d*). Similar swirls can also appear when an MHD flow has no recirculation. They arise due to the inertial force and destruction of Hartmann layers resulting from a decrease in the magnetic field, see Votyakov & Zienicke (2007).

The vertical drifts shown in figure 12(*b–d*) are caused by rotation of the fluid and can be understood as a manifestation of the hydrodynamic Ekman pumping effect, see e.g. Davidson (2001). There are six rotating columns in the MHD flow studied here, and each one has its own primary horizontal motion and secondary vertical drift. Taken together this gives rise to the helical motion clearly observed in figure 11.

The whole three-dimensional space trajectory for an infinitesimally small volume of fluid – a fluid particle – can now be described in the following way. Far upstream from the magnetic system, the particle moves in a straightline under the pressure gradient. Approaching the region of influence of the magnetic obstacle, the particle turns towards the closest corner owing to the action of the braking Lorentz force and reaches a boundary layer. If the particle is not captured by recirculation, it then passes the region of the magnetic obstacle in the bulk of two jets streamlined alongside the obstacle. If the particle is captured by recirculation, it first goes down (up) from the top (bottom) towards the middle plane in the helix of the magnetic vortex. In the middle plane, this trajectory joins the helix of the closest connecting vortex and passes helically towards the top (bottom) wall to reach again the boundary layer and dissipate the kinetic energy. Then, the particle can be caught by the helix of the attached vortex and drift slowly to the middle plane where it finally is free to go downstream from the magnet.

Recirculation under the magnetic poles brings new details into top and bottom boundary layers perpendicular to the magnetic field. These layers are Hartmann layers in the case of a constant magnetic field, Ekman layers in the case of an axisymmetric rotating flow bounded by a fixed horizontal plate, and Ekman–Hartmann layers when the axisymmetric rotating flow is subject to a constant vertical magnetic field, Acheson & Hide (1973), Desjardins, Dormy & Grenier (1999).[†] We checked the velocity profiles $u_x(z)$ in the region of magnetic vortices and found no satisfactory agreement with the present theory for Ekman–Hartman rotating flows. The reasons for this disagreement are probably that the recirculation induced by a heterogenous external magnetic

[†] We thank the referee who brought these works to our attention.

field shows details which are not compatible with the present analytic theory: (i) the rotating flow is not axisymmetric, (ii) neither magnetic field nor angular rotation are constant, (iii) this is a system of six rotating flows. The quantitative analysis of these layers requires further detailed investigation. At the moment we can conclude only that these layers are important to stabilize recirculation even at high Reynolds numbers as shown in next Section.

3.7. Recirculation in a three-dimensional flow versus vortex generation in a two-dimensional flow

This paper is devoted to a stationary three-dimensional MHD flow. Recently, Cuevas *et al.* (2006a) have reported vortex generation in a two-dimensional flow induced by a magnetic obstacle. In this Section, we discuss how their two-dimensional results are related to our three-dimensional results.

In our opinion, how to build a two-dimensional model at high Re is an open question. Two-dimensionality assumes that the flow rate is kept constant in the plane under consideration. This assumption is certainly wrong in the case of a local magnetic field, where Hartmann layers are formed (destroyed) under an inward (outward) magnetic field gradient, i.e. the streamwise velocity profile in the transverse direction is becoming more (less) flat, and therefore the fluid must go out of (go into) the plane, see discussion about given by Votyakov & Zienicke (2007) and their figures 8 and 9.

On one hand, the friction imposed by a no-slip wall stabilizes a flow because it provides a sink for kinetic energy. For instance, in hydrodynamics there are numerous experiments which illustrate that the confinement of the endplates increases the stability of a wake, see e.g. Shair *et al.* (1963), Nishioka & Sato (1974), Gerich & Eckelmann (1982), Lee & Budwig (1991). These examples include the delay of the critical Reynolds number for vortex shedding and the extension of the Reynolds number range for two-dimensional laminar shedding.

On the other hand, the case of an MHD flow under a local magnetic field always requires taking into account top and bottom endplates because these plates carry magnetic poles. In reality, one can increase the distance between poles to have more two-dimensionality in the middle plane, but this automatically decreases the degree of space heterogeneity of the external magnetic field. So, it becomes an issue whether it is practically possible to design a strongly heterogenous magnetic field having a large distance between magnetic poles.

There is a method to take no-slip top/bottom plates into consideration by means of the Hartmann friction term, see e.g. Lavrentiev *et al.* (1990). This has been used also by Cuevas *et al.* (2006a). However, this averaged approach is well validated only in the case of a small flow rate, i.e. low Re , even when the magnetic field is not strongly varying. It follows from the fact that past the magnetic obstacle the Hartmann friction takes the form of a Hele-Shaw friction based on the assumption that velocity is parabolic along the z -axis. This is well validated only for viscous flows where vorticity advection does not play a significant role, Riegels (1938). The formal vertical Hele-Shaw friction term inserted into the two-dimensional Navier–Stokes equations does not describe quantitatively the behaviour of the system with high Re . We believe that this friction has no significant influence when the advection is strong.

Nevertheless, one can consider mathematically what happens in a two-dimensional free (no sidewalls) MHD flow where the flow rate is kept constant. This mathematical problem has been addressed by Cuevas *et al.* (2006a).

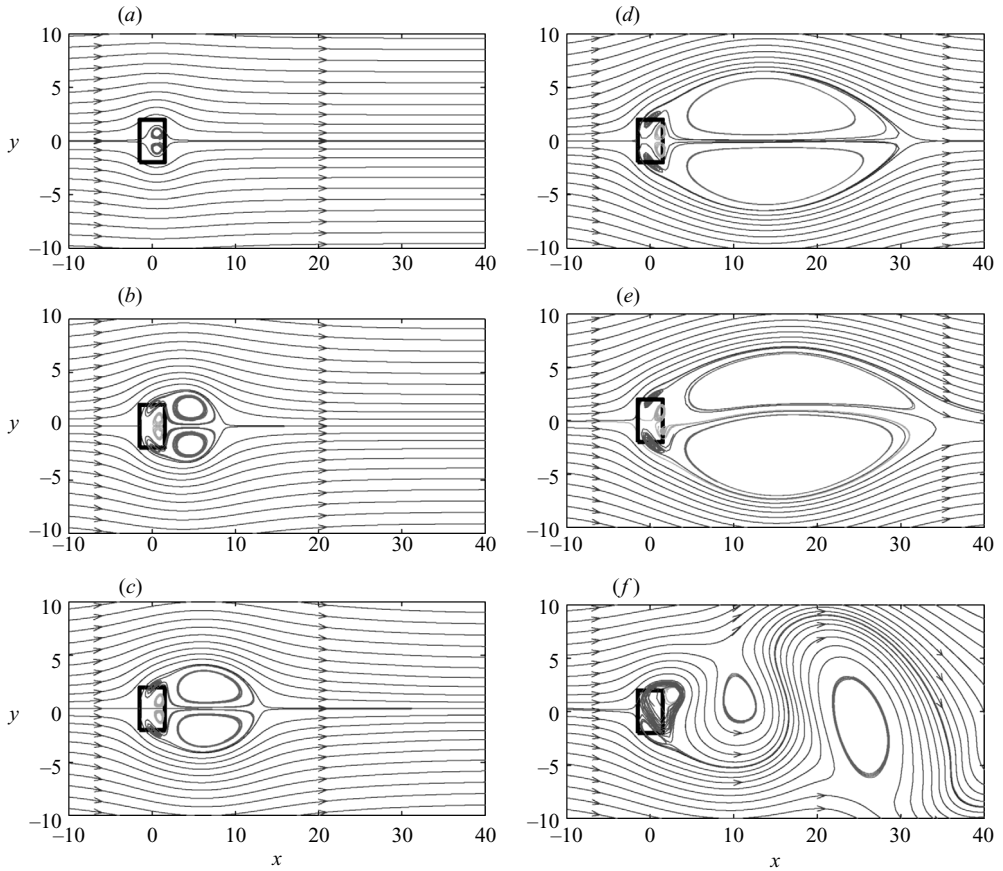


FIGURE 13. Flow streamlines in a two-dimensional non-steady free flow: (a) $t = 1$, (b) 10, (c) 20, (d) 90, (e) 120, (f) 150; $\mathbf{u}(\mathbf{r})|_{t=0} = (1.5, 0)$, $N = 30$, $Re = 100$.

This two-dimensional MHD flow had no walls and, hence, no sinks for kinetic energy except an internal viscosity which is negligible when Re is high. In such a flow, no vortex pattern can be stabilized, and one would not observe any stationary recirculation. Instead one obtains non-steady vortex generation; hence, it is worth discussing a developing flow, i.e. the flow starting from a constant velocity field $\mathbf{u}(\mathbf{r})|_{t=0} = (u_x, 0)$. We have performed a few runs of a two-dimensional simulation in order to reproduce results of Cuevas *et al.* (2006a) and find whether the six-fold vortex pattern shown in figure 1(b) is general. These results are presented in figure 13.

One observes, at the initial times, symmetric magnetic vortices (figure 13a), and then a six-vortex pattern (figure 13b, c). This pattern quickly grows in size due to inertia (figure 13b, c, d), in such a way that attached vortices gradually swell and reach a dimension much larger than that of magnetic and connecting vortices. When attached vortices exceed their critical size, they become unstable and lose symmetry, figure 13(e). This gives rise to the Kármán vortex street, figure 13(f), illustrated also by a vorticity contour plot in figure 14. The Kármán vortex street has been reported by Cuevas *et al.* (2006a), while the preceding temporal evolution, figure 13(a–f), is described here for the first time.

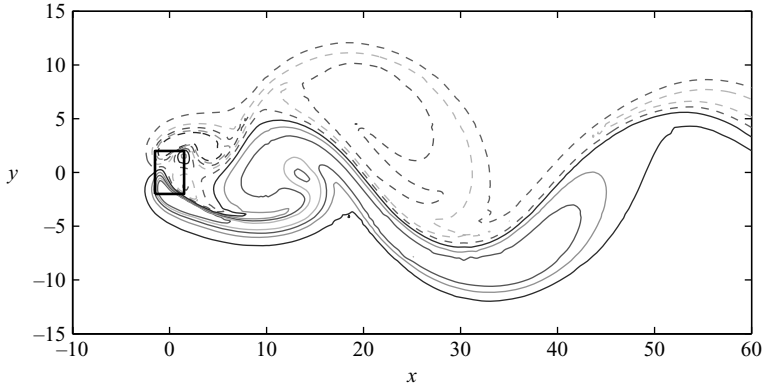


FIGURE 14. Vorticity field corresponding to figure 13(*f*) ($t = 150$), ($N = 9$, $Re = 100$). Dashed lines are plotted for negative vorticity, and solid lines are plotted for positive vorticity.

It is known that attached vortices in the flow past a solid body can be found at any Reynolds number Re at the initial instance of time before vortex shedding starts. One can see that the same situation takes place in an initial flow past the magnetic obstacle. The difference is that instead of just attached vortices one can also observe a six-fold vortex pattern developing from the recirculation under the magnetic gap.

4. Conclusions

We have reported the results of a three-dimensional numerical study on a stationary liquid metal flow in a rectangular duct under the influence of an external magnetic field. The interaction parameter N , Reynolds number Re as well as magnetic field configuration have been systematically varied. Whenever it has been possible, the numerical results have been quantitatively compared with experimental ones.

First, an analytical, physically consistent and simple model for the external magnetic field has been derived. Parameters of the model are the geometric dimensions of the region occupied by external magnets. This model has been successfully verified by comparing with experimentally measured data and then used in the paper by varying the constraint factor, $\kappa = M_y/L_y$, the ratio between spanwise dimension of the magnet, $2M_y$, and width of the duct, $2L_y$.

One can classify the flow structures into which a stationary MHD flow is organized into the following three typical categories, depending on the interaction parameter N as well as spanwise magnetic field heterogeneity.

The first structure, attributed to a low degree of field heterogeneity, is characterized by a significant electromotive force which opposes the electrostatic field. The characteristic pattern for this case is the Hartmann flow. If the magnetic field is uniform, this regime takes place at all N ; otherwise it is realized at the N where the field heterogeneity is not strong manifested.

The second stationary structure is perfectly observed for a fringing magnetic field, i.e. when the intensity of the transverse magnetic field is varied slowly in the spanwise and strongly in the streamwise direction. The flow pattern is given by an M-shaped streamwise velocity profile without recirculation inside the magnetic gap. Here, the

electromotive force and the electrostatic field can either be opposed or in the same direction, but the direction of the electromotive force is always in the direction of the electric current. The loops of the electric current are located mainly in the horizontal plane.

The decisive condition for the appearance of the third flow structure is a strong spanwise variation of the magnetic field which induces recirculation inside the magnetic obstacle. The recirculation starts when the reverse electrostatic field reaches a critical value. Here, the electromotive force is opposed to the electrostatic field and the direction of the electric current. For this recirculation regime, the intensities of the reverse flow, obtained in three-dimensions numerically and by physical experiments have been compared, and a good agreement has been observed.

The existence regions of stable stationary flow patterns, that is the dependence of the critical interaction parameter $N_{c,m}$ to induce recirculation on the constraint factor κ , has been calculated and discussed. It has been made clear that no recirculation is possible for a perfectly spanwise uniform external magnetic field. Moreover, the MHD flows for various κ have been shown to be similar provided they have the same ratio $N/N_{c,m}$.

Finally, three-dimensional features of the flow under consideration have been discussed and it has been demonstrated that the magnetic vortices have a stable disposition. This is contrary to a two-dimensional numerical study where stationary recirculation is possible only in a creeping flow while at higher flow rate the recirculation develops vortex shedding. Nevertheless, one can see all these vortex patterns in a two-dimensional non-steady flow at initial times.

We close this work with some hypotheses on the nature of the transitions that we have found in this system, namely, (i) the transition between streamlining flow and the flow with magnetic vortices when $N_{c,m}$ and κ are varied, and (ii) the transition from the two-vortex pattern (only magnetic vortices) to the six-vortex pattern (magnetic, connecting and attached vortices) when the Reynolds number is varied. The first transition has a high probability of being a topological change of the same solution, which is stable in the whole space of initial conditions. An increase of the strength as well as an increase or decrease of the spanwise inhomogeneity of the magnetic field seem us to be topological changes of the force field resulting in a topological change of the stationary stable solution. This would be consistent with the fact that we never found different flow patterns coexisting for the same parameter pair $(N_{c,m}, \kappa)$. The second transition mentioned is in our opinion analogous to the appearance of attached vortices behind a solid obstacle known from hydrodynamics. The magnetic vortices act as an obstacle for the flow. On increasing Reynolds number a shear instability arises resulting in the formation of attached vortices, which for consistency of the flow be accompanied by connecting vortices. These impressions on the questions of stability, that we gained from our research on the system considered, however, remain to be proved rigorously.

The authors express their gratitude to the Deutsche Forschungsgemeinschaft for financial support in the frame of the "Research Group Magnetofluidynamics" at the Ilmenau University of Technology under grant ZI 667. The simulations were carried out on a JUMP supercomputer, access to which was provided by the John von Neumann Institute (NIC) at the Forschungszentrum Jülich. We are grateful for many fruitful discussions with Andre Thess. Special thanks go to our experimental colleague Oleg Andreev, for an always close exchange of thoughts and for providing the experimental data to compare with our numerical results.

Appendix. Indefinite integrals

We use the following notation: $\mathbf{r} = (x, y, z)$, $\mathbf{r}' = (x', y', z')$, $\Delta r = |\mathbf{r} - \mathbf{r}'| = [\Delta x^2 + \Delta y^2 + \Delta z^2]^{1/2}$ and $\Delta x = x - x'$, $\Delta y = y - y'$, $\Delta z = z - z'$. Then, the indefinite integration over z' gives

$$\Phi^{(z)}(x, y, z, x', y', z') = \int \frac{dz'}{|\mathbf{r} - \mathbf{r}'|} = -\operatorname{arctanh} \left[\frac{\Delta z}{\Delta r} \right], \quad (\text{A } 1)$$

the indefinite integration over z', y' gives

$$\begin{aligned} \Phi^{(z,y)}(x, y, z, x', y', z') &= \int \frac{dy' dz'}{|\mathbf{r} - \mathbf{r}'|} = -\Delta x \operatorname{arctan} \left[\frac{\Delta y \Delta z}{\Delta x \Delta r} \right] \\ &\quad + \Delta y \operatorname{arctanh} \left[\frac{\Delta z}{\Delta r} \right] + \Delta z \operatorname{arctanh} \left[\frac{\Delta y}{\Delta r} \right], \end{aligned} \quad (\text{A } 2)$$

and finally the indefinite integration over z', y', x' gives

$$\begin{aligned} \Phi^{(z,y,x)}(x, y, z, x', y', z') &= \int \frac{dx' dy' dz'}{|\mathbf{r} - \mathbf{r}'|} \\ &= \frac{1}{2} \Delta x^2 \operatorname{arctan} \left[\frac{\Delta y \Delta z}{\Delta x \Delta r} \right] - \Delta y \Delta z \operatorname{arctanh} \left[\frac{\Delta x}{\Delta r} \right] \\ &\quad + \frac{1}{2} \Delta y^2 \operatorname{arctan} \left[\frac{\Delta x \Delta z}{\Delta y \Delta r} \right] - \Delta x \Delta z \operatorname{arctanh} \left[\frac{\Delta y}{\Delta r} \right] \\ &\quad + \frac{1}{2} \Delta z^2 \operatorname{arctan} \left[\frac{\Delta x \Delta y}{\Delta z \Delta r} \right] - \Delta x \Delta y \operatorname{arctanh} \left[\frac{\Delta z}{\Delta r} \right]. \end{aligned} \quad (\text{A } 3)$$

To confirm this, one can use a commercial program, e.g. Mathematica, to analytically differentiate (A 3) back and obtain (A 1) finally. The original way to calculate (A 1)–(A 3) is quite cumbersome, and is not provided here.

REFERENCES

- ACHESON, D. J. & HIDE, R. 1973 Hydromagnetics of rotating fluids. *Rep. Prog. Phys.* **36**, 159–221.
- AFANASYEV, Y. D. 2006 Formation of vortex dipoles. *Phys. Fluids* **18**, 037103.
- ALBOUSSIERE, TH. 2004 A geostrophic-like model for large Hartmann number flows. *J. Fluid Mech.* **521**, 125–154.
- ANDREEV, O., KOLESNIKOV, YU. & THESS, A. 2007 Experimental study of liquid metal channel flow under the influence of a non-uniform magnetic field. *Phys. Fluids* **19**, 039902.
- CUEVAS, S., SMOLENTSEV, S. & ABDOU, M. 2006a On the flow past a magnetic obstacle. *J. Fluid Mech.* **553**, 227–252.
- CUEVAS, S., SMOLENTSEV, S. & ABDOU, M. 2006b Vorticity generation in creeping flow past a magnetic obstacle. *Phys. Rev. E* **74**, 056301.
- DAVIDSON, P. 1999 Magnetohydrodynamics in Materials Processing. *Annu. Rev. Fluid Mech.* **31**, 273–300.
- DAVIDSON, P. A. 2001 *An Introduction to Magnetohydrodynamics*. Cambridge University Press.
- DESJARDINS, B., DORMY, E. & GRENIER, E. 1999 Stability of mixed Ekman-Hartmann boundary layers. *Nonlinearity* **12**, 181–199.
- GELFGAT, Y. M. & OLSHANSKII, S. V. 1978 Velocity structure of flows in non-uniform constant magnetic fields. ii. experimental results. *Magnetohydrodynamics* **14**, 151–154.
- GELFGAT, Y. M., PETERSON, D. E. & SHCHERBININ, E. V. 1978 Velocity structure of flows in nonuniform constant magnetic fields 1. numerical calculations. *Magnetohydrodynamics* **14**, 55–61.

- GERICH, D. & ECKELMANN, H. 1982 Influence of end plates and free ends on the shedding frequency of circular cylinders. *J. Fluid Mech.* **122**, 109–121.
- GRIEBEL, M., DORNSEIFER, T. & NEUNHOEFFER, T. 1995 *Numerische Strömungssimulation in der Strömungsmechanik*. Vieweg.
- JACKSON, J. D. 1999 *Classical Electrodynamics*, 3rd Edn Wiley.
- KIT, L. G., PETERSON, D. E., PLATNIEKS, I. A. & TSINOBER, A. B. 1970 Investigation of the influence of fringe effects on a magnetohydrodynamic flow in a duct with nonconducting walls. *Magnetohydrodynamics* **6**, 485–491.
- KUNSTREICH, S. 2003 Electromagnetic stirring for continuous casting – Part 1. *Rev. Met. Paris* **100**, 395–408.
- LAURENTIEV, I. V., MOLOKOV, S. YU., SIDORENKOV, S. I. & SHISHKO, A. YA 1990 Stokes flow in a rectangular magnetohydrodynamic channel with nonconducting walls within a nonuniform magnetic field at large Hartmann numbers. *Magnetohydrodynamics* **26**, 328–338.
- LEE, T. & BUDWIG, R. 1991 A study of the effect of aspect ratio on vortex shedding behind circular cylinders. *Phys. Fluids* **3**, 309–315.
- MOREAU, R. 1990 *Magnetohydrodynamics*. Kluwer.
- NISHIOKA, M. & SATO, H. 1974 Measurements of velocity distributions in the wake of a circular cylinder at low Reynolds numbers. *J. Fluid Mech.* **65**, 97–112.
- RIEGELS, F. 1938 Zur Kritik des Hele-Shaw-Versuchs. *Z. Angew. Math. Mech.* **18** (2), 95–106.
- ROBERTS, P. H. 1967 *An Introduction to Magnetohydrodynamics*. Longmans, Green.
- SHAIR, F. H., GROVE, A. S., PETERSEN, E. E. & ACRIVOS, A. 1963 The effect of confining walls on the stability of the steady wake behind a circular cylinder. *J. Fluid Mech.* **17**, 546–550.
- SHERCLIFF, J. A. 1962 *The Theory of Electromagnetic Flow-measurement*. Cambridge University Press.
- STERL, A. 1990 Numerical simulation of liquid-metal MHD flows in rectangular ducts. *J. Fluid Mech.* **216**, 161–191.
- TAKEUCHI, S., KUBOTA, J., MIKI, Y., OKUDA, H. & SHIROYAMA, A. 2003 Change and trend of molten steel flow technology in a continuous casting mould by electromagnetic force. In *Proc. EPM-Conference*. Lyon, France.
- TANANAEV, A. B. 1979 *MHD duct flows*. Moscow: Atomizdat.
- THESS, A., VOTYAKOV, E. V. & KOLESNIKOV, Y. 2006 Lorentz Force Velocimetry. *Phys. Rev. Lett.* **96**, 164501.
- VOROPAYEV, S. I. & AFANASYEV, Y. D. 1994 *Vortex Structures in a Stratified Fluid*. Chapman and Hall.
- VOTYAKOV, E. V., KOLESNIKOV, Y., ANDREEV, O., ZIENICKE, E. & THESS, A. 2007 Structure of the wake of a magnetic obstacle. *Phys. Rev. Lett.* **98**, 144504.
- VOTYAKOV, E. V. & ZIENICKE, E. 2007 Numerical study of liquid metal flow in a rectangular duct under the influence of a heterogeneous magnetic field. *Fluid Dyn. Mater. Process.* **3** (2), 97–113.